Data reduction of the Ground-based CO data: Technical report

Padelis Papadopoulos[1], Paul van der Werf[2,3], Kate Isaak[4], E. M. Xilouris[5]

[1]Max Planck Institute für Radioastronomie, Auf dem Hügel 69, D-53121 Bonn, Germany
[2]Leiden Observatory, Leiden University, PO Box 9513, NL-2300 RA Leiden, the Netherlands
[3]SUPA, Institute for Astronomy, University of Edinburgh, Royal Observatory, Blackford Hill, Edinburgh EH9 3HJ
[4]Research and Scientific Support Department, European Space Agency, Keplerlaan 1, 2200 AG Noordwijk, the Netherlands
[5]Institute for Astronomy, Astrophysics, Space Applications & Remote Sensing, National Observatory of Athens, P. Penteli, 15236 Athens, Greece

THE OBSERVATIONS

We used the A3 receiver (211–276 GHz, DSB operation) on the 15-m JCMT on Mauna Kea in Hawaii (USA) to observe the CO J =2–1 (230.538 GHz) and ^{13}CO J =2–1 (220.398 GHz) lines, and its B3 (315–370 GHz) and W/C (430–510 GHz) receivers operating single sideband (SSB) for CO J = 3–2 (345.796 GHz) and J = 4–3 (461.041 GHz) line observations in our sample. The observations were conducted during several periods from 1999 up to 2010 (see Table 1 for specific periods and typical system temperatures). CO J = 3–2 observations beyond 2008 utilized the new 16-beam HARP-B SSB receiver (325–375 GHz). The decommissioning of the W/C JCMT receiver before completion of the survey as well as the several CO J = 4–3 lines redshifted into the deep 450-GHz atmospheric absorption band meant that such measurements could be conducted for only 10 out of the original sample of 30 LIRGs. The digital autocorrelation spectrometer (DAS) was used in all JCMT observations until 2006, while the new spectrometer ACSIS was employed afterwards. At 345 GHz we used its 920-MHz (~800 km/s) or 1.8-GHz (~1565 km/s) bandwidth mode, depending on the expected line width and the need for maximum sensitivity (i.e. when 920-MHz bandwidth was sufficient to cover the line, dual-channel operation was possible with B3 and was used for better sensitivity). For the high-frequency W/C observations, the widest 1.8-GHz bandwidth was used throughout whose ~1170 km/s velocity coverage adequately covered the full width at zero intensity (FWZI) of all the CO 4–3 lines observed. For the CO, ^{13}CO J = 2–1 lines both bandwidth modes were used, yielding ~1200– 2345 km/s velocity coverage. Beam switching with frequencies of $\nu_{\rm chop}$ =1–2 Hz, at throws of 120–180 arcsec (in azimuth) ensured flat baselines. The beam sizes were HPBW(230 GHz) = 22 arcsec, HPBW(345 GHz) = 14 arcsec and HPBW(461 GHz) = 11 arcsec. We checked and updated the pointing model offsets every hour using continuum and spectral line observations of strong sources, with average residual pointing rms scatter $\sigma_{\rm r} = \sqrt{\sigma_{\rm el}^2 + \sigma_{\rm az}^2} \lesssim 2.5$ arcsec.

The CO J = 6–5 observations

The first measurements of the CO J = 6–5 line (691.473 GHz) were conducted for the luminous ULIRG/QSO Mrk 231 and the LIRG Arp 193 in our sample using the old JCMT W/D band (620–710 GHz) receiver (operating in SSB mode) on 2005 February 20 and April 22, respectively, under excellent, dry conditions ($\tau_{220\,\rm GHz} \leq 0.035$). The typical system temperatures were $T_{\rm sys}$ ~ (3700–5500)K (including atmospheric absorption). The DAS spectrometer was used in its widest mode of 1.8 GHz (~780 km/s at 690 GHz), and beam switching at frequencies of $\nu_{\rm chop}$ =2 Hz with azimuthal throws of 60 arcsec resulted in flat baselines. The beam size at 691 GHz was HPBW=8 arcsec. Good pointing with such narrow beams is crucial and was checked every 45–60 min using differential pointing with the B3 receiver (350 GHz). This allows access to many more suitable compact sources in the sky than direct pointing with theW/D receiver at 690 GHz, and was found accurate to within $\sigma_{\rm r}$ ~ 2.6 arcsec (rms) during that observing period. The other CO J = 6–5 measurements were conducted during 2009, with the upgraded W/D receiver equipped with new SIS mixers (effectively the same type installed at the Atacama Large Milimeter Array (ALMA) telescopes in this waveband) which dramatically enhanced its performance. The resulting low receiver temperatures ($T_{\rm rx}$ ~550 K) allowed very sensitive observations with typical $T_{\rm sys}$ ~ 1500–3000K (including atmospheric absorption) for $\tau_{220\,\rm GHz}$ ~ 0.035–0.06. Dual channel operation (after the two polarization channels were aligned to within_1 arcsec) further enhanced theW/Dband observing capabilities at the JCMT (see Table 1).

Table 1. JCMT: observing periods, CO lines and typical system temperatures.

Year	Periods	Spectral lines	T_{sys} (K)[a]
1999	July 6–20	CO 3–2, 4–3	450–700 (B3), 1130–2380 (W/*C*)
2001	December 10–28	CO 3–2	380–550 (B3)
2002	February 24–25	CO 3–2	630–690 (B3)
2002	April 17–18	CO 3–2	760, 1100–1700 (B3)
2002	June 17–30	CO 2–1, 3–2	550 (A3), 430–650, 900–1200 (B3)
2002	November 20–23	CO 4–3	2600–4800, 6000–9300 (W/*C*)[b]
2003	November 6	CO 3–2	4000–4400 (B3)
2004	January 20	CO 3–2	530–620 (A3)
2004	April 2 to May 29	^{12,13}CO 2–1, CO 3–2	300–450 (A3), 470–2400 (B3)[b]
2004	July 13 to August 25	^{12,13}CO 2–1, CO 3–2	320–510 (A3), 800–1000 (B3)
2004	September 28 to November 10	^{12,13}CO 2–1, CO 3–2	300–600 (A3), 530–1350 (B3)
2004	November 18	CO 4–3	2450–2800 (W/*C*)
2005	February 20	CO 6–5	4500–5200 (W/*D*)
2005	April 17–23	CO 3–2, 4–3, 6–5	720–1100 (B3), 1600 (W/*C*), 3700–5500 (W/*D*)
2005	August 22	^{13}CO 2–1	415–420 (A3)
2005	October 10–28	^{12,13}CO 2–1	230–420 (A3)
2005	December 15–31	^{12,13}CO 2–1, CO 3–2	330–490 (A3), 750–980 (B3)
2006	December 15–18	^{13}CO 2–1	250–280 (A3/ACSIS)
2007	December 16–21	^{13}CO 2–1	230–280 (A3/ACSIS)
2007	February 22–24	^{13}CO 2–1	310–320 (A3/ACSIS)
2008	May 9	CO 3–2	1630 (HARP-B/ACSIS)
2009	January 6–7	CO 6–5	2600–3200, 7500 (W/*D*, ACSIS)[b]
2009	January 22–25	CO 6–5	1700–2600, 9000 (W/*D*, ACSIS)[b]
2009	February 1	CO 6–5	2200–3500 (W/*D*, ACSIS)
2009	January 27	CO 6–5	2000–2900 (W/*D*, ACSIS)
2009	March 2	CO 6–5	1300–1500 (W/*D*, ACSIS)
2009	January 13–15	CO 6–5	1900–3100 (W/*D*, ACSIS)
2010	September 11	CO 6–5	1400–1800 (W/*D*, ACSIS)

[a] T_{sys} values include atmospheric absorption. High values of T_{sys}(B3) $\gtrsim$ 600 K and T_{sys}(A3) $\gtrsim$ 350 K) are measured in a few cases close to tuning range limits (ν_{sky} < 320 GHz for B3 and $\nu_{sky} \leq$ 215 GHz for A3), or when $|\nu_{sky} - 325\,\mathrm{GHz}| < 5$ GHz, i.e. close to a strong atmospheric absorption feature at 325 GHz.
[b] The high T_{sys} values found only for VIIZw 31, a circumpolar source at the JCMT latitude, observed at elevation of $\sim 30°$.

The ACSIS spectrometer at its widest mode of 1.8 GHz was used, while in a few cases two separate tunings were used to create an effective bandwidth of ~3.2 GHz (~1390 km s^{-1} at 690 GHz) so that it adequately covers (U)LIRG CO lines with FWZI ~ 800–950 km/s. Rapid beam switching at ν_{chop} = 4 Hz (continuum mode) and azimuthal throw of 30 arcsec yielded very flat baselines under most circumstances. The pointing model was updated every 45–60 min using observations of compact sources with the W/*D* receiver, as well as differential pointing with the A3 receiver, yielding rms residual error radius of σ_r ~ 2.2 arcsec. The final CO *J* = 6–5 observations were conducted in 2011 during which I Zw1 was observed, with only one W(*D*) receiver channel functioning, under dry conditions ($\tau_{220\,\mathrm{GHz}} \leq 0.05$) that yielded T_{sys} ~ 1400–1800 K. The same beam-switching scheme was used, while two separate tunings yielded an effective bandwidth of ~3.2 GHz covering the wide CO line of this ULIRG/QSO (e.g. Barvainis, Alloin & Antonucci 1989). The pointing uncertainty remained within the range of previous CO *J* = 6–5 observations. Nevertheless, we wish to note that isolated cases of large pointing offsets reducing the observed CO *J* = 6–5 line fluxes have been found (e.g. for Arp 220; see P10a and P10b) and may have affected a few of these highly demanding CO line

The IRAM 30-m observations

Observations of CO, ^{13}CO *J* = 1–0 and 2–1 with the IRAM 30- m telescope were conducted during two sessions in 2006, namely from June 20 to 25 and from November 26 to 28. In both periods, the A100/B100 (3 mm) and A230/B230 (1 mm) receivers were used, connected to the 1-MHz (A100/B100, 512 MHz) and 4-MHz (A230/B230, 1 GHz) filter banks. During the first period, the A230/B230 receivers were used to observe the ^{12}CO *J* = 2–1 line. If the latter was strong and detected in about an hour or less, the 1-mm receivers were then retuned to

^{13}CO J = 2–1. For sources with very weak ^{12}CO lines (e.g. 08030+5243 and 08572+3915), no attempt of observing ^{13}CO J = 2–1 was made. Data were acquired under new control system in a series of 4-min scans, each comprising eight 30-s subscans. The typical system temperatures (including atmospheric absorption) for the CO 2–1 observations were T_{sys}(210–230 GHz) ~ (220–500) K, with the lowest mostly during the ^{13}CO observations (though for occasional tunings towards the edge of the band and/or bad weather conditions T_{sys} ~ 700–900 K). For most sources, data were acquired in two or more different days to ensure a line detection and as a consistency check. Pointing and focus were checked frequently during the observations with residual pointing errors σ_r ~ 3 arcsec (rms). During the November period receivers A100/B100 were used to observe ^{13}CO J = 1–0 line simultaneously to the ^{12}CO J = 2–1 line observed with A230/B230 (tuned to the same line each time). The pointing error stayed ≤ 3 arcsec (rms), except during November 26 when it went up to ~6 arcsec (corresponding data were omitted). The typical system temperatures were T_{sys}(110 GHz)~110–160 K, T_{sys}(115 GHz)~200–380Kand T_{sys}(210–230 GHz)~330–425 K. Finally, in order to maintain very flat baselines, the wobbler switching (nutating subreflector) observing mode with a frequency of 0.5 Hz and beam throws of 180–240 arcsec was employed during both observing sessions. The beam sizes were HPBW(110 GHz) = 22 arcsec and HPBW(210–230 GHz) = 11 arcsec, with corresponding beam efficiencies[2] of B_{eff}(110 GHz) = 0.75, B_{eff}(230 GHz) = 0.52 and B_{eff}(210 GHz) = 0.57, and forward beam efficiencies of F_{eff}(3 mm) = 0.95 and F_{eff}(1 mm)=0.91.We also note that in most cases we had redundant CO J = 2–1 measurements with the JCMT, and then adopted (a) the average when JCMT/IRAM values agreed to within 20 per cent (most cases) or (b) the JCMT measurement (as its wider beam is less prone to flux loss due to pointing offsets and/or beam-throw/flux-loss uncertainties) if a discrepancy larger than the aforementioned was found.

Table 2. Point source S_ν/T (Jy/K) conversion factors and HPBW values used for the observations and literature data.

Telescope[a]	110–115 GHz[b]	210–230 GHz	315–345 GHz[b]	430–461 GHz[b]	620–710 GHz[b]
IRAM 30 m (S_ν/T_A^*)	6.3[c] (22 arcsec)	7.9, 8.7 (11 arcsec)			
JCMT (S_ν/T_A^*)		25–28 (22 arcsec)	28–38 (14 arcsec)	50–74 (11 arcsec)	49–62 (8 arcsec)
NRAO 12 m (S_ν/T_R^*)	35[d] (55 arcsec)	55 (32 arcsec)			
FCRAO 14 m (S_ν/T_A^*)	42 (45 arcsec)[e]				
Onsala 20 m (S_ν/T_A^*)	31 (33 arcsec)				
SEST (S_ν/T_{mb})	27 (45 arcsec)[f]	41(22 arcsec)[f]			
HHSMT (S_ν/T_{mb})			50[g] (23 arcsec)		
NRO 4 m (S_ν/T_{mb})	2.4[h] (14.5 arcsec)				
CSO (S_ν/T_{mb})			43[i] (21 arcsec)		

[a]The telescope and temperature scale type (see Kutner & Ulich 1981 for definitions).
[b]The frequency range per receiver.
[c]For $T_A^* = (B_{eff}/F_{eff}) \times T_{mb} = 0.789 \times T_{mb}$: $S_\nu/T_{mb} = 4.95$ Jy/K, used to obtain the CO 1–0 fluxes from all the IRAM 30-m spectra in the literature that are reported in the T_{mb} scale (unless a different S_ν/T_{mb} is mentioned).
[d]Measured at 110 GHz (Section 2.3.2), also in the NRAO 12-m User's Manual 1990 edition, fig. 14.
[e]The T_R^* scale is sometimes used to report data from the FCRAO 14 m (e.g. Sanders et al. 1986), for which $S_\nu/T_R^* = \eta_{fss}\left(S_\nu/T_A^*\right) = 31.5$(Jy/K) (for $\eta_{fss} = 0.75$) is adopted.
[f]http://www.ls.eso.org/lasilla/Telescopes/SEST/html/telescopeinstruments/telescope/index.html.
[g]The Heinrich Hertz Submillimeter Telescope (Arizona, USA) (from Narayanan et al. 2005).
[h]For the NRO 45-m telescope in Nobeyama (Japan) at 115 GHz: $\Gamma = (8k_B/\pi D^2)(\eta_{mb}/\eta_a)$ and adopting $\eta_a = 0.32$, $\eta_{mb} = 0.44$ (from the NRO website).
[i]Caltech Submillimeter Observatory (CSO): $\Gamma = (8k_B/\pi D^2)(\eta_{mb}/\eta_a)$, where $D = 10.4$ m, $\eta_{mb} = 0.746$ and $\theta_{1/2} = 1.22(\lambda/D)$, yielding $\eta_a/\eta_{mb} = 0.76$ (using $\Omega_A A_c = \lambda^2$ and $\eta_a = A_c/A_g$, $\eta_{mb} = \Omega_{mb}/\Omega_A$).

DATA REDUCTION AND LINE INTENSITY ESTIMATES

In both telescopes the output spectra are in the T_A* scale (see Kutner & Ulich 1981). We inspected all individual 10/4–6 min JCMT/IRAM spectra for baseline ripples and to clip any intensity 'spikes' in individual channels. The edited spectra were then co-added using a $1/\sigma^2$-weighting scheme and linear baselines were subtracted from each final co-added spectrum. These spectra are shown in Figs 1 and 2 and were used to derive the velocity-integrated molecular line flux densities from

$$\begin{aligned} S_{\rm line} &= \int_{\Delta V} S_\nu \, {\rm d}V = \frac{8k_{\rm B}}{\eta_{\rm a}^* \pi D^2} K_{\rm c}(x) \int_{\Delta V} T_{\rm A}^* \, {\rm d}V \\ &= \frac{\Gamma({\rm Jy/K})}{\eta_{\rm a}^*} K_{\rm c}(x) \int_{\Delta V} T_{\rm A}^* \, {\rm d}V, \end{aligned} \tag{1}$$

Table 3. Observational parameters of the combined LIRG sample.

Name[a]	RA (J2000)[b]	Dec. (J2000)[b]	z ($D_{\rm L}$)[c]	($\Delta\theta_\alpha$, $\Delta\theta_\delta$)[d] (arcsec, arcsec)	$\langle\theta_s\rangle$[e] (arcsec)	References[f]
00057+4021	00 08 20.58	+40 37 55.5	0.0445 (194.5)	(0, 0)	0.81 (co)	$1^{p,m}$
00322−0840* (NGC 157)	00 34 46.48	−08 23 47.8	0.0055 (23.3)	(0, 0)	80 (co,sm,x)	$2^{p,m}$
00509+1225 (I Zw 1, PG 0050+124)	00 53 34.92	+12 41 35.5	0.0611 (270.3)	(0, 0)	$\lesssim$12 (co)	3^{m},4^{p}
01053−1746* (Arp 236)	01 07 47.00	−17 30 24.0	0.0200 (85.8)	(0, 0)	30 (sm,x)	5^{p},6^{m}
01077−1707*	01 10 08.20	−16 51 11.0	0.0351 (152.3)	(0, 0)	$\lesssim$15 (sm)	5^{p},6^{m}
01418+1651* (III Zw 35)	01 44 30.50	+17 06 08.0	0.0274 (118.2)	(0, 0)	$\lesssim$15 (sm)	5^{p},6^{m}
02071+3857 (NGC 828, VI Zw 177)	02 10 09.43	+39 11 26.3	0.0178 (76.2)	(0, 0)	14 (co)	$7^{p,m}$,8^{m}
02080+3725* (NGC 834)	02 11 01.55	+37 40 01.3	0.0154 (65.8)	(− 2.5, −2.0)	13 (cm)	9^{p},10^{m}
02114+0456* (Mrk 1027)	02 14 05.60	+05 10 27.7	0.0297 (128.3)	(0, 0)	17 (sm,x)	5^{p},6^{m}
02321−0900 (NGC 985, Mrk 1048)	02 34 37.74	−08 47 14.7	0.0430 (187.7)	(0, 0)	22 (co)	$11^{p,m}$
02401−0013* (NGC 1068)	02 42 40.74	−00 00 47.6	0.0037 (13.3)	(0, 0)	40 (co,sm,x)	$12^{p,m}$
02483+4302	02 51 36.01	+43 15 10.8	0.0514 (225.8)	(0, 0)	1.75 (co)	$1^{p,m}$
02512+1446* (UGC 2369)	02 54 01.80	+14 58 14.0	0.0312 (135.0)	(0, 0)	30 (sm,cm,x)	5^{p},6^{m},13^{m}
03359+1523	03 38 46.90	+15 32 55.0	0.0353 (153.2)	(0, 0)	4.5 (cm)	5^{p},13^{m}
04232+1436	04 26 04.94	+14 43 37.9	0.0796 (356.4)	(−1.13, +0.4)	$\lesssim$8 (cm,sm,x)	14^{p},6^{m},13^{m}
05083+7936 (VII Zw 031)	05 16 46.51	+79 40 12.5	0.0543 (239.0)	(0, 0)	2.3 (co)	$1^{p,m}$
05189−2524	05 21 01.11	−25 21 45.9	0.0427 (186.4)	(+ 4.0, +1.0)	$\lesssim$3 (cm,ir)	9^{p},15^{m},13^{m}
08030+5243	08 06 50.10	+52 35 05.4	0.0835 (375.4)	(0, 0)	$\lesssim$0.8 (ir)	14^{p},16^{m}
08354+2555* (NGC 2623, Arp 243)	08 38 24.10	+25 45 16.5	0.0185 (79.3)	(0, 0)	1.65 (co)	$17^{p,m}$
08572+3915[g]	09 00 25.41	+39 03 54.1	0.0582 (256.9)	(0, 0)	$\lesssim$2.1 (co)	$18^{p,m}$
09126+4432 (Arp 55)	09 15 54.90	+44 19 54.4	0.0399 (173.3)	(0, 0)	1.9, 12 (co,cm,dbl)	5^{p}, 13^{m},19^{m}
09320+6134 (UGC 05101)	09 35 51.53	+61 21 11.6	0.0393 (171.1)	(0, 0)	1,−2 (ir,co)	14^{p},15^{m},20^{m}
09586+1600* (NGC 3094)	10 01 26.00	+15 46 14.0	0.0080 (34.0)	(−2.2, −1.0)	11 (ir,cm)	21^{p},22^{m},13^{m}
10039−3338* (IC 2545)	10 06 04.50	−33 53 03.0	0.0341 (147.9)	(0, 0)	$\lesssim$15 (sm)	5^{p},6^{m}
10035+4852	10 06 45.83	+48 37 46.1	0.0648 (287.5)	(+ 5.2, +2.2)	$\lesssim$15 (sm)	14^{p},6^{m}
10173+0828	10 20 00.19	+08 13 34.5	0.0489 (214.4)	(0, 0)	$\lesssim$3 (co,cm)	$23^{p,m}$,13^{m}
10190+1322	10 21 42.60	+13 06 54.4	0.0765 (342.2)	(0, 0)	1.2, 4 (co,dbl)	$24^{p,m}$
10356+5345* (NGC 3310)	10 38 45.90	+53 30 11.7	0.0033 (14.0)	(0, 0)	50 (co,sm,x)	$2^{p,m}$
10565+2448	10 59 18.15	+24 32 34.4	0.0428 (188.2)	(0, 0)	1.5 (co)	$1^{p,m}$
11191+1200 (PG 1119+120)	11 21 47.12	+11 44 18.3	0.0500 (219.4)	(0, 0)	$\lesssim$5 (co)	$25^{p,m}$
11231+1456* (IC 2810, UGC 6436)	11 25 45.00	+14 40 36.0	0.0341 (147.9)	(+1.2, 0)	6 (cm,sm)	21^{p},13^{m},26^{m}
11257+5850 (Arp 299)	11 28 32.45	+58 33 45.8	0.0103 (43.8)	(0, 0)	35 (co,sm,x)	$27^{p,m}$,6^{m}
12001+0215* (NGC 4045)	12 02 42.30	+01 58 38.0	0.0066 (28.0)	(−0.9, −1.2)	7 (cm)	21^{p},13^{m}
12112+0305	12 13 45.77	+02 48 39.3	0.0727 (324.4)	(+3.9, +2.1)	$\lesssim$2 (2.9) (co,dbl)	9^{p},18^{m}
12224−0624*	12 25 03.90	−06 40 53.0	0.0263 (113.4)	(0, 0)	$\lesssim$2 (cm)	21^{p},13^{m}
12243-0036* (NGC 4418)	12 26 54.70	−00 52 39.0	0.0073 (31.0)	(0, 0)	$\lesssim$3 (cm)	21^{p},13^{m}
12540+5708 (Mrk 231)	12 56 14.21	+56 52 25.1	0.0422 (184.1)	(0, 0)	0.85 (co)	$1^{p,m}$
13001−2339*	13 02 52.10	−23 55 19.0	0.0215 (92.3)	(0, 0)	2 (ir)	5^{p},22^{m}
13102+1251* (NGC 5020)	13 12 39.90	+12 35 59.0	0.0112 (47.7)	(−1.0, −0.9)	12 (cm)	21^{p},13^{m}
Arp 238* (UGC 08335)	13 15 30.20	+62 07 45.0	0.0315 (136.3)	(0, 0)	5 (35) (cm,dbl)	5^{p}, 10^{m}
13183+3423 (Arp 193)	13 20 35.32	+34 08 22.2	0.0233 (100.2)	(0, 0)	1.5 (co)	$1^{p,m}$
13188+0036* (NGC 5104)	13 21 23.10	+00 20 32.0	0.0186 (79.7)	(0, 0)	2.5 (cm)	21^{p},13^{m}
13229−2934 (NGC 5135)	13 25 43.97	−29 50 01.3	0.0136 (58.0)	(0, 0)	6 (cm)	$10^{p,m}$
13362+4831 (NGC 5256)	13 38 17.90	+48 16 41.0	0.0278 (120.0)	(0, 0)	8 (cm, sm)	5^{p},13^{m},6^{m}
13428+5608 (Mrk 273)	13 44 42.12	+55 53 13.5	0.0378 (164.4)	(0, 0)	3 (co)	$1^{p,m}$
13470+3530* (UGC 8739)	13 49 14.20	+35 15 23.0	0.0168 (71.9)	(−2.5, +1.5)	11 (cm,x)	21^{p},13^{m}
F13500+3141 (3C 293)	13 52 17.82	+31 26 46.4	0.0446 (194.9)	(0, 0)	7 (co)	$28^{p,m}$
F13564+3741* (NGC 5394)	13 58 33.60	+37 27 13.0	0.0125 (53.3)	(0, 0)	5 (cm)	21^{p},13^{m}
14003+3245* (NGC 5433)	14 02 36.00	+32 30 38.0	0.0145 (61.9)	(0, 0)	8.5 (cm)	21^{p},13^{m}
14151+2705* (Mrk 673)	14 17 21.00	+26 51 28.0	0.0366 (159.0)	(0, 0)	$\lesssim$10 (opt)	$5^{p,m}$
14178+4927* (Zw 247.020, Mrk 1490)	14 19 43.20	+49 14 12.0	0.0256 (110.3)	(0, 0)	2 (cm)	21^{p},13^{m}
14280+3126* (NGC 5653)	14 30 10.40	+31 12 54.0	0.0119 (50.7)	(−2.0, +1.6)	17 (cm)	21^{p}, 13^{m}
14348−1447	14 37 38.32	−15 00 22.7	0.0825 (370.7)	(0, 0)	$\lesssim$2, 3.5 (co,dbl)	$29^{p,m}$,13^{m}
15107+0724 (Zw 049.057)	15 13 13.07	+07 13 32.0	0.0129 (55.0)	(0, 0)	5 (co)	$23^{p,m}$
15163+4255* (Mrk 848, Zw 107)	15 18 06.20	+42 44 42.0	0.0402 (175.1)	(0, 0)	7 (sm,cm)	5^{p}, 6^{m}, 13^{m}
15243+4150* (NGC 5930, Arp 090)	15 26 07.90	+41 40 34.0	0.0089 (37.8)	(0, 0)	2.5 (cm)	21^{p},13^{m}
15322+1521* (NGC 5953p, Arp 091)	15 34 32.30	+15 11 38.0	0.0065 (27.6)	(0, 0)	10 (cm)	21^{p},13^{m}
15327+2340 (Arp 220)	15 34 57.24	+23 30 11.2	0.0182 (78.0)	(0, 0)	1.8 (co)	$1^{p,m}$
15437+0234* (NGC 5990)	15 46 16.50	+02 24 56.0	0.0128 (54.6)	(−2.1, −0.8)	11 (cm)	21^{p},13^{m}
16104+5235* (NGC 6090, Mrk 496)	16 11 40.70	+52 27 25.0	0.0292 (126.1)	(0, 0)	6 (cm)	5^{p},13^{m}
16284+0411* (MCG +01-42-008)	16 30 56.50	+04 04 59.0	0.0245 (105.5)	(0, 0)	3.9 (cm)	21^{p},13^{m}
16504+0228 (NGC 6240)	16 52 59.05	+02 24 05.8	0.0243 (104.6)	(0, 0)	3 (co)	7^{p},30^{m}

Table 3 – *continued*

Name[a]	RA (J2000)[b]	Dec. (J2000)[b]	z (D_L)[c]	($\Delta\theta_\alpha$, $\Delta\theta_\delta$)[d] (arcsec, arcsec)	$\langle\theta_s\rangle$[e] (arcsec)	References[f]
17132+5313	17 14 20.48	+53 10 31.4	0.0507 (222.6)	(0, +1.0)	2.4 (cm)	31^{p},13^{m}
17208−0014	17 23 21.92	−00 17 00.7	0.0428 (186.8)	(0, 0)	1.7 (co)	$1^{p,m}$
18425+6036* (NGC 6701)	18 43 12.27	+60 39 10.5	0.0132 (56.3)	(+1.5, +2.0)	15 (cm)	9^{p},10^{m}
19458+0944	19 48 15.47	+09 52 01.3	0.1000 (454.8)	(0, 0)	$\lesssim$0.8 (ir)	14^{p},16^{m}
20550+1656* (II Zw 96)	20 57 23.70	+17 07 44.0	0.0363 (157.7)	(0, 0)	20 (sm,x)	5^{p},6^{m}
22491−1808	22 51 49.86	−17 52 24.4	0.0773 (346.0)	(−7.3, 0)	2.5 (ir,cm,x)	9^{p},15^{m},13^{m}
23007+0836 (NGC 7469)	23 03 15.60	+08 52 26.3	0.0163 (69.7)	(0, 0)	8 (co)	$32^{p,m}$
23365+3604	23 39 01.25	+36 21 08.4	0.0644 (285.6)	(0, 0)	0.95 (co)	$1^{p,m}$

[a] *IRAS* name and the most common alternative(s), the asterisk marks sources for which CO line fluxes were obtained from an extensive literature search and line flux rectification process (see Sections 2 and 4.2).
[b] Source coordinates ($R_{\rm beam}$) used for CO observations.
[c] The redshift used for receiver tuning (or the $z_{\rm co}$ reported in the literature for LIRGs not in the original sample), and the corresponding luminosity distance in Mpc.
[d] Offsets between expected CO source centre $R_{\rm cm}$ (assumed coincident with peak cm continuum) and observed position: $\Delta R = R_{\rm cm} - R_{\rm beam}$ ($\Delta R = 0$ when available CO or submm images defined the CO source centre, see Section 4.2). Thus $R_{\rm cm}$ marks the true CO source centre whenever $\Delta R \neq 0$.
[e] CO region angular size $\langle\theta_s\rangle = (\theta_{\rm min}\theta_{\rm maj})^{0.5}$, from interferometric maps. If these were not available, then cm, near-IR or submm continuum images were used to set upper limits on $\langle\theta_s\rangle$. The qualifiers for the images used are (co), (cm), (ir), (sm) for CO, cm, IR and submm images, (x) = complex source morphology ($\langle\theta_s\rangle$ then denotes the overall source size), (dbl) = double CO-bright nuclei. In the latter case, $\langle\theta_s\rangle$ refers to the largest one, and the second number denotes their separation.
[f] References used for source position (= p) and morphology/size (= m) information: 1 – DS98; 2 – Zhu et al. (2009); 3 – Schinnerer, Eckart & Tacconi (1998); 4 – Eckart et al. (1994); 5 – Leech et al. (2010); 6 – Mortier et al. (private communication); 7 – Wang et al. (1991); 8 – Casoli, Durpaz & Combes (1992); 9 – Sanders et al. (1991); 10 – Condon et al. (1996); 11 – Appleton et al. (2002); 12 – Papadopoulos & Seaquist (1999); 13 – Condon et al. (1990); 14 – Solomon et al. (1997); 15 – Scoville et al. (2000); 16 – Murphy et al. (1996); 17 – Bryant & Scoville (1999); 18 – Evans et al. (2002); 19 – Sanders et al. (1988a); 20 – Wilson et al. (2008); 21 – Yao et al. (2003); 22 – Zenner & Lenzen (1993); 23 – Planesas et al. (1991); 24 – Graciá-Carpio, Planesas & Colina (2007); 25 – Evans et al. (2001); 26 – Lisenfeld et al. (2000); 27 – Aalto et al. (1997); 28 – Evans et al. (1999); 29 – Evans, Surace & Mazzarella (2000); 30 – Tacconi et al. (1999); 31 – Young et al. (1995); 32 – Davies, Tacconi & Genzel (2004); 33 – Crawford et al. (1996).
[g] Double nuclei in near-IR (Scoville et al. 2000), but only one is CO bright (Evans et al. 2002).

where $\Gamma_{\rm JCMT}$ = 15.62, $\Gamma_{\rm IRAM}$ = 3.905 and η^*_a is the aperture efficiency defined against the T_A^* scale [$\eta^*_a = \eta_a/\eta_{\rm rss}$, where η_a is the aperture efficiency measured against the T_A scale, as is more typical, and $\eta_{\rm rss}$ is the rearward spill over and scattering efficiency; equations (8.16) and (8.17) in Rohlfs & Wilson 1996]. The factor $K_c(x) = x^2/(1 - e^{-x^2})$, with $x = \theta_s/(1.2\theta_{\rm HPBW})$ and θ_s is the source diameter, accounts for the geometric coupling of the beam (its Gaussian part) to a disc-like source, when a CO emission size was available, and $2\sigma_r \leq \theta_s$ _ $\theta_{\rm HPBW}$, where σ_r is the pointing error radius (see Section below). The total point source conversion factors S_ν/T adopted for the JCMT, the IRAM 30-m telescope and all the data gleaned from the literature (for the corresponding output antenna temperature scales) is comprehensively tabulated in Table 2.

Aperture efficiencies, line intensity uncertainties and biases

Aperture efficiencies of large high-frequency submm telescopes such as the JCMT can change significantly (especially for $\nu \geq$460 GHz) depending on a variety of factors (e.g. elevation, thermal relaxation of the dish or its reshaping after an holography session). In order to track them over a decade of observations (during which the JCMT dish has been readjusted quite a few times), we conducted frequent aperture efficiency measurements using planets and adopted the average η^*_a obtained per observing period for deriving the line fluxes of all the sources observed during it. In many cases, as a cross-check, we distributed the measurements of very CO-luminous LIRGs over several widely separated periods, during which very different aperture efficiencies (sometimes up to a factor of~2) were often measured. In all such cases, equation (1), with the appropriate η^*_a values, yielded velocity-integrated line fluxes in excellent agreement among each other. Indicatively most aperture efficiencies measured for the JCMT lay within $\eta^*_a \sim$ 0.41–0.56 (*B* band, 315–350 GHz) and $\eta^*_a \sim$ 0.21–0.31 (*C* band, 430–461 GHz). For the three periods of the more demanding W/*D* band observations, we derived η^*_a = 0.25 (2005), η^*_a = 0.32 (2009) and η^*_a = 0.27 (2010) from planetary measurements. The uncertainties for the reported velocity-integrated line flux densities have been computed from

$$\frac{\Delta S_{\rm line}}{S_{\rm line}} = \left[\left(\frac{\delta T_{\Delta V}}{T_{\Delta V}}\right)^2_{\rm th} + \left(\frac{\delta T_{\Delta V}}{T_{\Delta V}}\right)^2_{\rm cal} + \left(\frac{\delta\eta}{\eta}\right)^2\right]^{1/2}, \qquad (2)$$

where $\delta T_{\_V}$ is the stochastic error of the average line intensity $T_{\_V}$ (averaged over the line FWZI ΔV), η is the telescope efficiency factor (used to derive the integrated line flux from the temperature scale of the output spectrum, e.g. η^*_a for T^*_A and $\delta\eta$ its uncertainty. The first term is estimated from the spectra shown in Figs 1 and 2 using

$$\left(\frac{\delta T_{\Delta V}}{T_{\Delta V}}\right)_{\rm th} = \frac{\delta T_{\rm chan}}{T_{\Delta V}}\left(\frac{N_{\Delta V}+N_{\rm bas}}{N_{\Delta V}N_{\rm bas}}\right)^{1/2}, \qquad (3)$$

where $\delta T_{\rm chan}$ is the stochastic intensity dispersion, estimated from the line-free part of the spectrum (for a given velocity channel width $\Delta V_{\rm chan}$), while $N_{\Delta V} = \Delta V/\Delta V_{\rm chan}$ and $N_{\rm bas} = 2\Delta V_{\rm bas}/\Delta V_{\rm chan}$ are the number of channels within the line FWZI and the line-free baseline (with $\Delta V_{\rm bas}/\Delta V_{\rm chan}$ channels symmetrically around the line), respectively. The second term in equation (2) accounts for line calibration errors (due to a host of factors such as imprecise knowledge of the calibration loads, uncertainties in the atmospheric model and the derived extinction, etc.). Observations of numerous strong spectral line standards and planets during each observing period yielded intensity dispersions of ~15 per cent (230 and 345 GHz), ~20 per cent (460 GHz) and ~25 per cent (690 GHz), which we adopt as the combined calibration (cal) and $\delta\eta/\eta$ uncertainties per observing band at the JCMT. For the 30-m observations we consider these to be ~15 per cent for both 3- and 1-mm bands. Finally, even with the accurate tracking and pointing achievable by enclosed telescopes such as the JCMT, the residual rms pointing errors and the narrow beams of large mm/submm telescopes at high frequencies can lead to a substantial and systematic reduction of measured fluxes of compact sources. We try to account for this as described in P10a by applying a $\langle G\rangle$ scaling factor to the line fluxes of all point-like sources with CO emission region diameters of $\theta_{\rm co} \le 2\sigma_{\rm r}$ [where $\sigma_{\rm r}$(JCMT) = 2.5 arcsec and $\sigma_{\rm r}$(IRAM) = 3 arcsec are the pointing error radii]. This factor is (see P10a)

$$G(\sigma_{\rm r}) = 1 + 8\ln 2\left(\frac{\sigma_{\rm r}}{\sqrt{2}\,\theta_{1/2}}\right)^2, \qquad (4)$$

where $\theta_{1/2}$ is the half power beam width (HPBW) and $\sigma_{\rm r}/\sqrt{2}$ is the rms pointing error per pointing coordinate. For $\theta_{\rm co} \le 2\sigma_{\rm r}$, $K_{\rm c}(x)$ is replaced in equation (1) by $G(\sigma_{\rm r})$ as the beam–source coupling correction is overtaken by the pointing error correction. At 345 and 460 GHz for the JCMT, we obtain $\langle G_{345}\rangle$=1.087 and $\langle G_{460}\rangle$=1.15, (with negligible correction at 230 GHz), while for 30 m $\langle G_{230}\rangle$= 1.20 (and negligible correction at 115 GHz). The CO J =6–5 observations with HPBW~8 arcsec are the most susceptible to this bias and _G_{690} has been estimated from the pointing rms *per observing session*, yielding a range _G_{690} = 1.17–1.37. For sources with CO (or submm dust emission) sizes of $2\sigma_{\rm r}$ _ $\theta_{\rm s}$ _ $\theta_{1/2}$, the $K_{\rm c}$ factor is used in equation (1). Finally, in the cases where large offsets were found between the presumed CO source centre and the observed positions in the literature (see discussion in Section 4.2), we applied a beam-shift correction factor of $K_{\rm sh}$ = exp [4 ln 2($\Delta\theta$/ HPBW)^2], where $\Delta\theta$ is the (beam centre)–source offset.

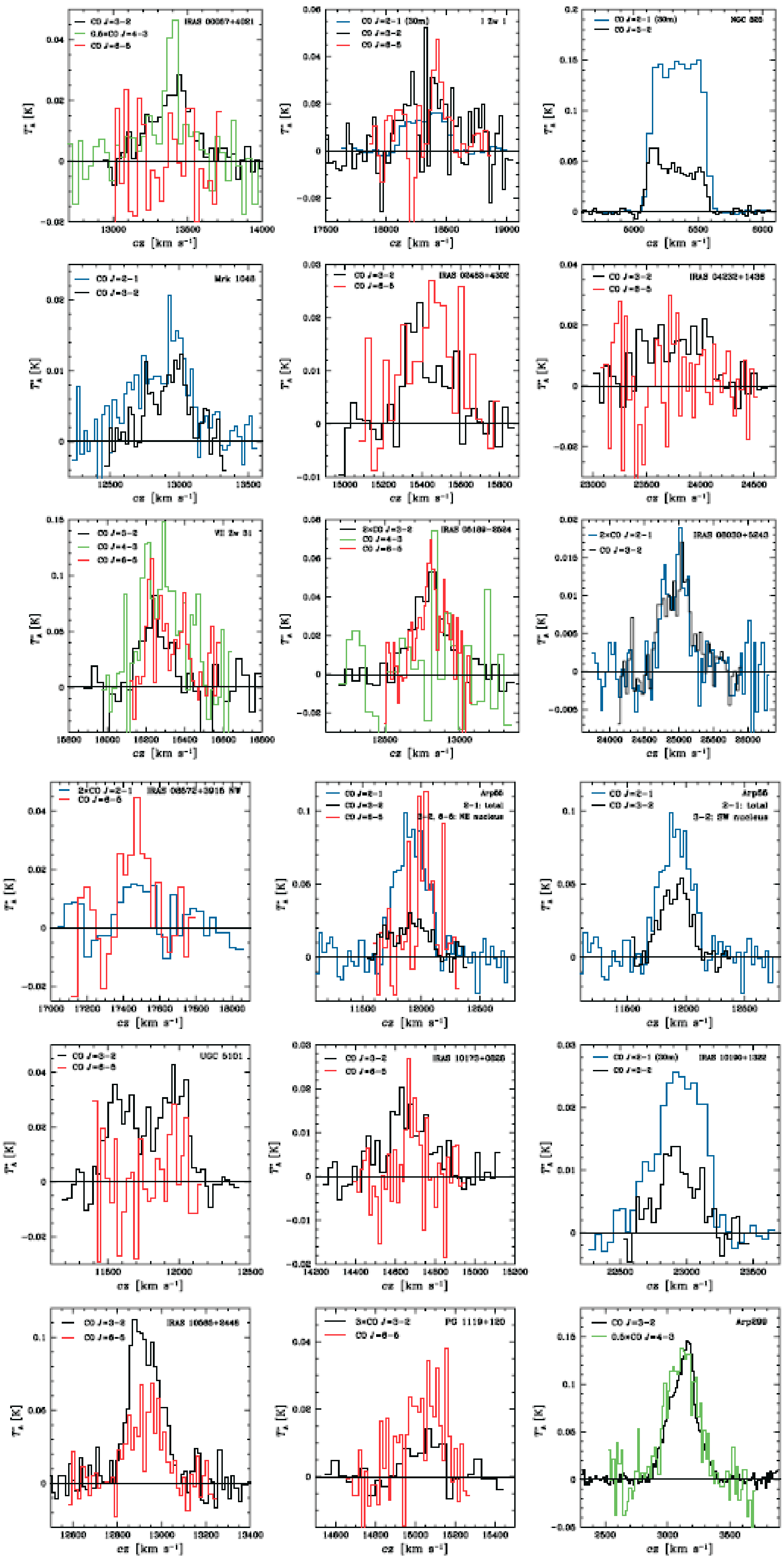

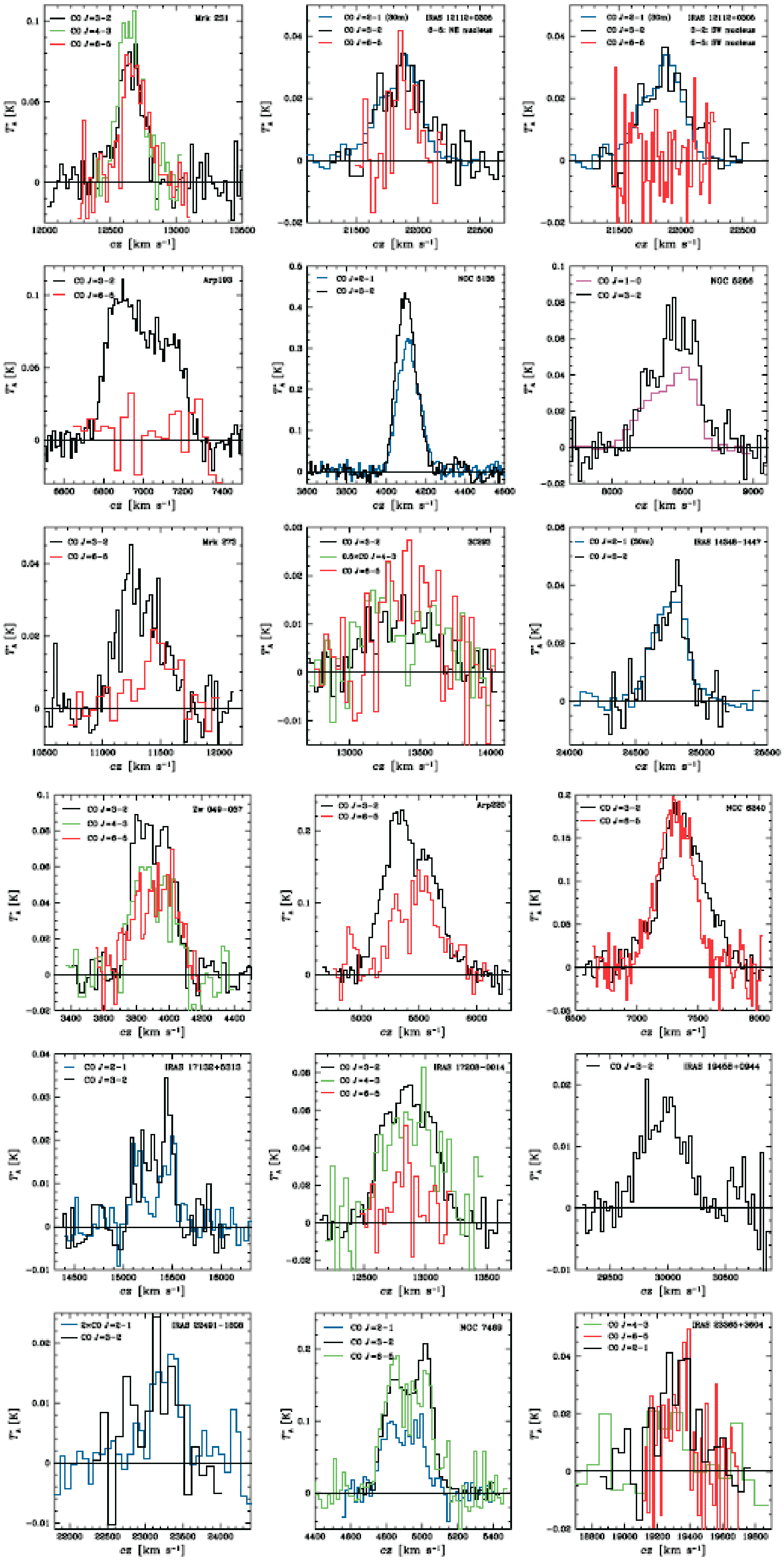

Figure 1. The high-J CO J+1→J, J+1≥3 spectra. In the few cases where all three CO J=3-2, 4-3 and 6-5 lines are available we omit the overlay of CO J=2-1 in order to reduce confusion (the J=2-1 lines are all shown in Fig. 2). The velocities are with respect to $V_{opt}=cz_{co}$ (LSR), and with typical resolutions ΔV_{ch}~10-50 km/s. A common colour designated per transition is used in all frames.

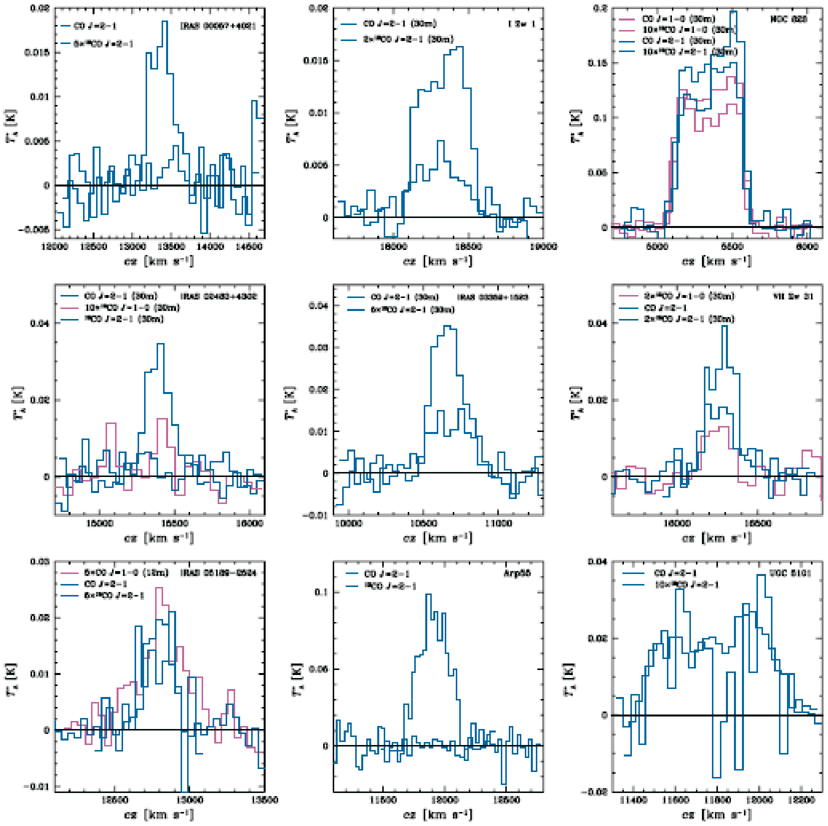
I Zw 1
NGC 828
VII Zw 31
Arp55
UGC 5101

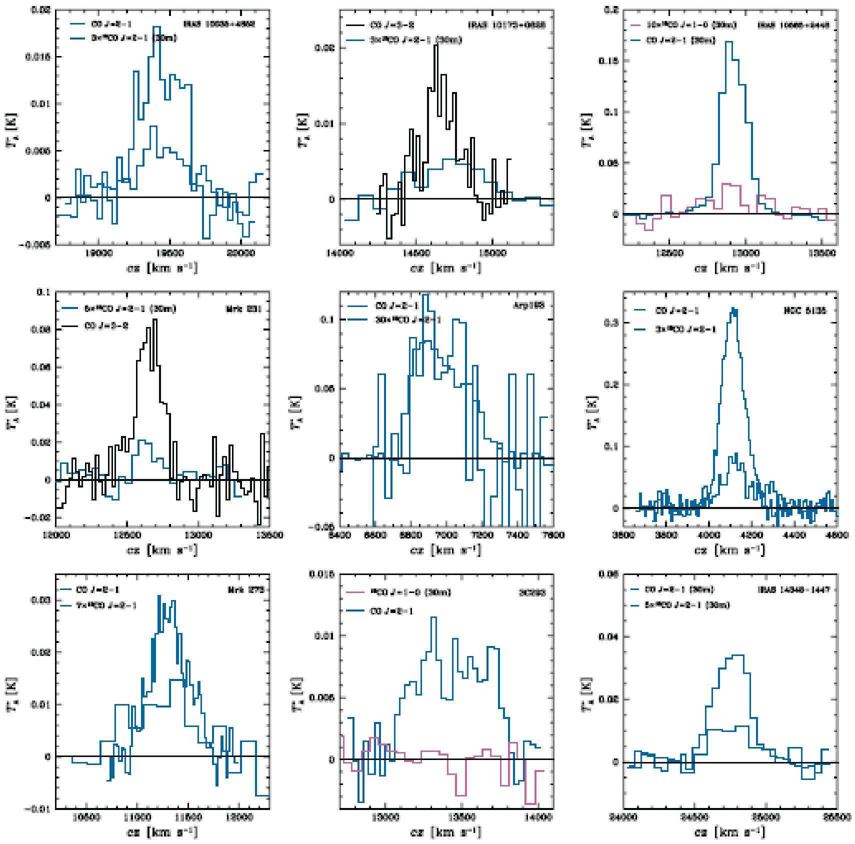
Mrk 231
Arp193
NGC 5135
Mrk 273
3C293

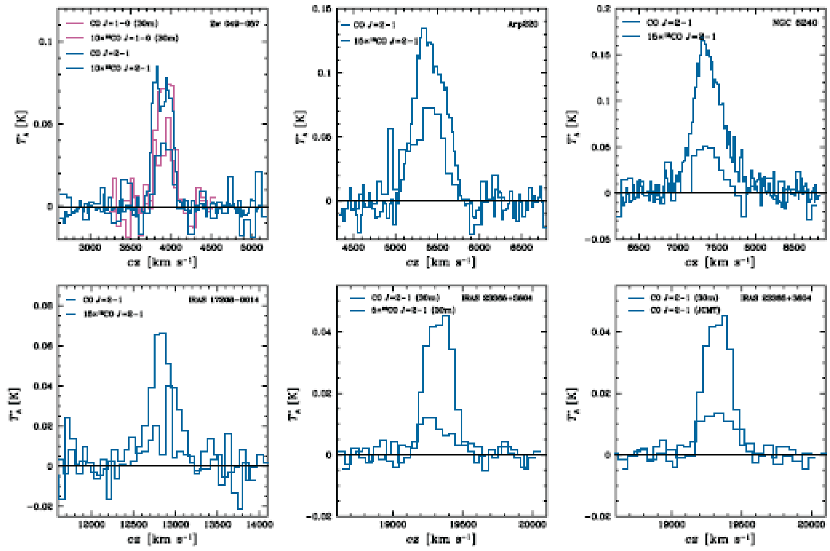

Figure 2. The CO, ^{13}CO line data. The velocities are with respect to $V_{opt}=cz_{co}$ (LSR), and with typical resolutions ΔV_{ch} ~(35-90) km/s. A common colour designated per transition is used in all frames.

Acknowledgements: The authors gratefully acknowledge financial support under the "DeMoGas" project. The project "DeMoGas" is implemented under the "ARISTEIA" Action of the "OPERATIONAL PROGRAMME EDUCATION AND LIFELONG LEARNING" and is co-funded by the European Social Fund (ESF) and National Resources.